Ultrafast Science
A SCIENCE PARTNER JOURNAL

RESEARCH ARTICLE

Ultrafast Optomechanical Terahertz Modulators Based on Stretchable Carbon Nanotube Thin Films

Maksim I. Paukov[1*], Vladimir V. Starchenko[1], Dmitry V. Krasnikov[2], Gennady A. Komandin[3], Yuriy G. Gladush[2], Sergey S. Zhukov[1], Boris P. Gorshunov[1], Albert G. Nasibulin[2], Aleksey V. Arsenin[1,4], Valentyn S. Volkov[1], and Maria G. Burdanova[1,5*]

[1]Center for Photonics and 2D Materials, Moscow Institute of Physics and Technology, Dolgoprudny, Russia. [2]Skolkovo Institute of Science and Technology, Moscow, Russia. [3]Prokhorov General Physics Institute of the Russian Academy of Sciences, Moscow, Russia. [4]Laboratory of Advanced Functional Materials, Yerevan State University, Yerevan, Armenia. [5]Institute of Solid State Physics of the Russian Academy of Sciences, Chernogolovka, Russia.

*Address correspondence to: paukov.mi@phystech.edu (M.I.P.); burdanova.mg@mipt.ru (M.G.B.)

Citation: Paukov MI, Starchenko VV, Krasnikov DV, Komandin GA, Gladush YG, Zhukov SS, Gorshunov BP, Nasibulin AG, Arsenin AV, Volkov VS, Burdanova MG. Ultrafast Optomechanical Terahertz Modulators Based on Stretchable Carbon Nanotube Thin Films. *Ultrafast Sci.* 2023;3:Article 0021. https://doi.org/10.34133/ultrafastscience.0021

Submitted 12 December 2022
Accepted 19 February 2023
Published 27 March 2023

For terahertz wave applications, tunable and rapid modulation is highly required. When studied by means of optical pump–terahertz probe spectroscopy, single-walled carbon nanotube (SWCNT) thin films demonstrated ultrafast carrier recombination lifetimes with a high relative change in the signal under optical excitation, making them promising candidates for high-speed modulators. Here, combination of SWCNT thin films and stretchable substrates facilitated studies of the SWCNT mechanical properties under strain and enabled the development of a new type of an optomechanical modulator. By applying a certain strain to the SWCNT films, the effective sheet conductance and therefore modulation depth can be fine-tuned to optimize the designed modulator. Modulators exhibited a photoconductivity change of approximately 2 times of magnitude under the strain because of the structural modification in the SWCNT network. Stretching was used to control the terahertz signal with a modulation depth of around 100% without strain and 65% at a high strain operation of 40%. The sensitivity of modulators to beam polarization is also shown, which might also come in handy for the design of a stretchable polarizer. Our results give a fundamental grounding for the design of high-sensitivity stretchable devices based on SWCNT films.

Introduction

The application of terahertz radiation has been found in many spheres including explosive and concealed weapon detection [1], medicine [2], pharmacy [3], etc. Since the beginning of the century, terahertz waves have also been considered as a means of wireless data transfer, which possess much better operation properties than current gigahertz and microwave technologies [4]. Several substantial advantages of terahertz communication are mentioned in [5]: increased bandwidth capacity, small diffraction of waves in free space, ability to provide secure communication, a small atmospheric scintillation effect, and low attenuation of terahertz radiation under weather conditions [6]. Terahertz modulation is a critical factor, which also has to be considered in developing ultrafast terahertz 6G technologies, in addition to generation, propagation, and detection [5].

The amplitude of terahertz waves passed through a medium is determined by its conductivity. Therefore, the electrical, optical, or thermal [7] manipulation of the conductivity provides a way to control the amplitude of terahertz radiation. The quality of typical modulators is characterized by several parameters, among which are modulation depth (MD) and modulation speed (MS). It has been reported that traditional bulk semiconductors, such as GaAs, Ge, and Si, can have either high MD and low MS (in order of several nanoseconds) [7] or fast MS (in order of several picoseconds) and insufficient MD (<40%) under the optical excitation [8]. Compared to 3-dimensional (3D) counterparts, optically controlled low-dimensional materials, such as graphene, transition metal dichalcogenides, carbon nanotubes (CNT), and nanowires, have demonstrated superior MD of up to 99% and MS of up to 600 GHz [9]. Electrically tuned modulators, based on low-dimensional materials, such as GaAs/AlGaAs and GaN/AlGaN nanoheterostructures [10,11], and monolayer graphene [9], also possess a giant MD factor of 93% to 99%.

Meanwhile, stretchable terahertz modulators with high efficiency are rarely observed. The MD of modulators based on 2D materials was rather small because of limited change in

conductivity under applied mechanical deformation [12,13]. This problem can be overcome using single-walled CNT (SWCNT) films, which have shown a great potential in optoelectronics [14,15], especially in stretchable devices [16]. SWCNTs are an easily manufactured nanomaterial with unique optical and electronic properties [17]. First, it has controllable strong excitonic absorption in visible and near-infrared ranges arising from the quasi-1D structure. Second, efficient charge carrier transport results in high terahertz conductivity [17]. This combination of efficient optical absorption and high charge mobilities makes SWCNT an ideal candidate for optically controlled terahertz modulation. In addition, SWCNTs have been already proved to have simultaneously high MD (up to 80%) and MS (up to 450 GHz) [18]. In addition, CNTs have also been proposed as one of the ideal candidates for terahertz modulation combining both high MS and MD. In [18], we showed that these fruitful results are due to the negative terahertz photoconductivity effect under optical excitation, which is widely studied nowadays [19]. Finally, some practical results involving stretchable CNT modulators have been reported [20]. It is worth mentioning that mechanical modulation in such devices may become one more degree of freedom to set the required MD and MS. On the whole, these arguments make stretchable SWCNT films more preferable and beneficial for terahertz applications than its counterparts.

In this work, we report the study on the influence of stretching on optically controlled modulators based on SWCNT. The designed modulators exhibit a photoconductivity change of approximately 2 times under 40% stretching, which can be used to control the terahertz optical modulator with giant initial MD close to 100%. To evaluate the possible explanation for the MD change under the applied strain, we discuss the possible mechanisms of photoconductivity change such as partial alignment, consequent formation of bundles [21], and formation of microcracks. The proposed tunable modulator paves a path for devices capable of switching the desirable properties of the terahertz signal.

Materials and Methods

Sample preparation

SWCNTs were synthesized by aerosol chemical vapor deposition method based on the carbon monoxide disproportionation (the Boudouard reaction) on the surface of Fe-based catalyst [22,23]. To prepare a thin film, The filtration of SWCNT aerosol with a nitrocellulose membrane was followed by the dry transfer on the transparent stretchable substrate: 0.2-mm-thick elastomer (Silpuran, Wacker) [24]. Two types of SWCNT films with thicknesses of approximately 11 and 106 nm (which correspond to optical transmittance of 90% and 60% at 550-nm wavelength, respectively) were obtained. All the thin films consisted of nearly equilibrium compositions: one-third metallic and two-thirds semiconducting SWCNTs [25].

Experimental design

The SWCNT film on the elastomer is placed between 2 jaws of the homemade mechanical stretcher with the ability to control elongation precisely. The film and its holder were placed horizontally and vertically into the spectrometers so that the light beam polarization was perpendicular and parallel according to the stretching direction. Raman spectra were obtained using a confocal microspectrometer (Labram, Jobin-Yvon Horiba) with a 532-nm laser at 0.58-mW power (spectral resolution of 2 cm^{-1} and spatial resolution of 1.5 mm).

The pump beam for the optical pump, terahertz probe (OPTP) spectroscopy was created using an optical parametric amplifier (TOPAS), seeded by a 1-kHz, 40-fs, 800-nm pulse (from a Newport Spectra Physics Spitfire ACE) to create pulses with a tunable center wavelength. Here, a pump wavelength of 600 nm was used. This wavelength corresponds to pump energy above the SWCNT bandgap and therefore matches their excitonic absorption lines [18]. As the used SWCNTs have narrow bandgaps, any wavelength shorter than 2.5 μm can be applied. The probe beam was generated using homemade conventional terahertz time–domain spectroscopy setup as described in [26], allowing us to measure both equilibrium conductivity and photoconductivity. The extraction of conductivity and photoconductivity was performed according to our previous study [27].

Results

Concept

The morphology of the SWCNT network changes under strain [16], which leads to the modification of optoelectronic properties (Fig. 1). Therefore, we would like to describe first the possible changes in the film that occur over the stretching. Stretching in one direction results in the alignment of SWCNT [16]. This consequently alters carrier conduction pathways, making it longer in the direction parallel to stretching because of the movement of SWCNT junctions and shorter in the perpendicular direction. Here and further, we use a term "conduction pathways" to describe both the interaction between free charges and the change of the percolation of the CNT network. To evaluate the anisotropy toward terahertz radiation, we have calculated the factor $Re(\sigma_{\perp})/\ Re(\sigma_{\parallel})$, where $Re(\sigma_{\perp})$ and $Re(\sigma_{\parallel})$ are the values of photoconductivity, which were obtained at the frequency of 1 THz for different relative elongations. The results are presented in Fig. S1. The reduction of the perpendicular component in comparison to the parallel component of the real part of the photoconductivity is present in the stretching direction, while the opposite behavior was observed in the compression direction. This indicates the gradual alignment and crack formation process that irreversibly modify the effective conductivity of the CNT network.

The further increase of stretching results in bundling primarily because of the reduced spacing between the SWCNTs. It has been reported that the conductivity of the SWCNT bundle is lower for bigger diameter bundles of SWCNTs [28]. The significant stretching results in the formation of microcracks. A strong relationship between resistance and these crack lengths has already been shown in dc measurements in [29]. The significant resistance increase was observed there because of the shortening of conductivity pathways in the direction parallel to stretching. In the same direction, cracks on individual SWCNT appeared due to the applied stresses. These factors also limit conductivity pathways but on a nanometer scale. Finally, the partial alignment causes the difference in the conductivity and photoconductivity in parallel and perpendicular directions in reference to the terahertz polarization beam because of the depolarization effect, according

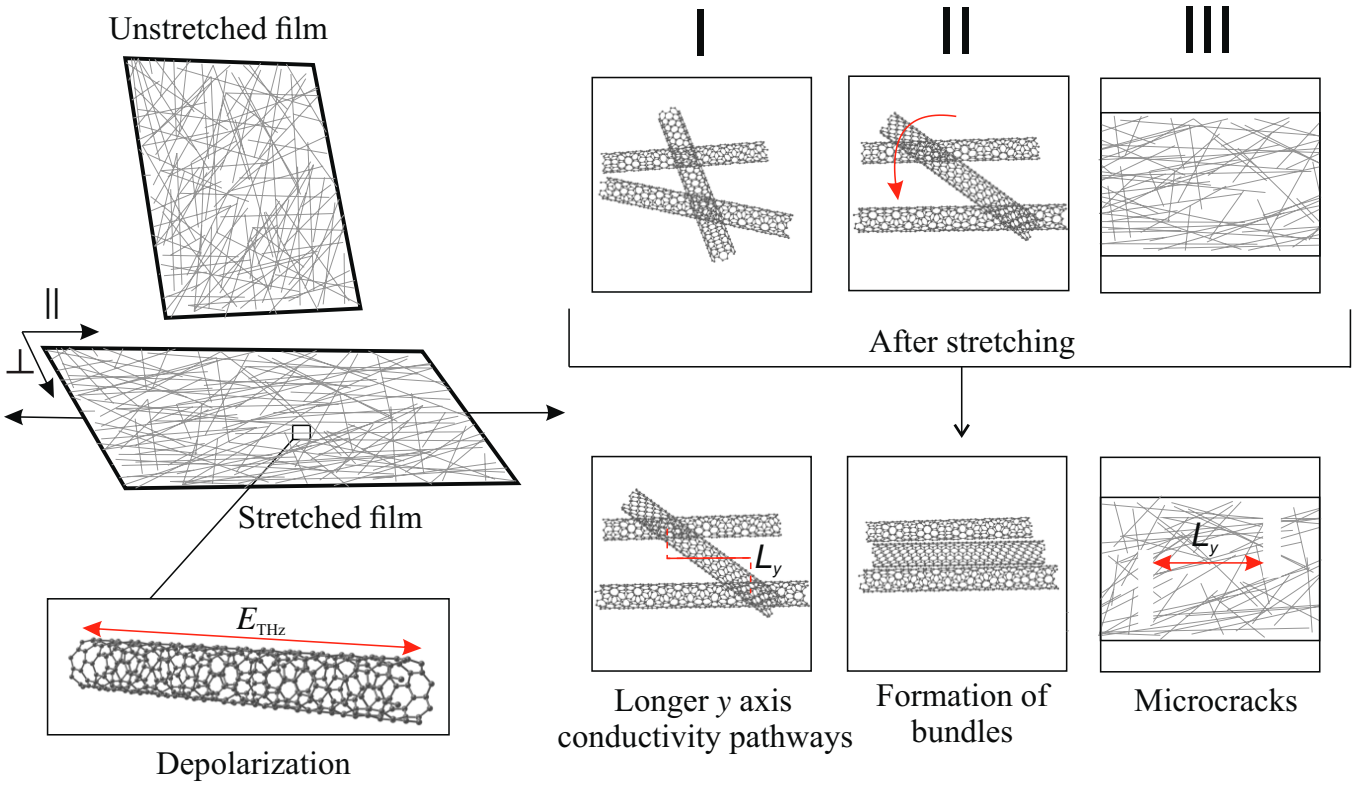

Fig. 1. Illustration of typical changes of single-walled carbon nanotube (SWCNT) film morphology formed by stretching. The stretching results in the following: I. Junction movement and partial alignment of SWCNT under strain. II. Formation of bundles due to the close location of aligning SWCNT. III. Formation of microcracks under applied stresses. Two typical experiments were performed—perpendicular and parallel to stretching and following compression directions. The partial alignment results in anisotropic properties coming from the depolarization effect.

to which optical absorption is suppressed when the polarization of the incident radiation is perpendicular to the SWCNT axis [30].

Photoconductivity change on stretching

In our previous studies [18,27], we showed that SWCNT thin films exhibit giant negative terahertz photoconductivity associated with the trion formation under optical excitation, which results in the uniquely high MD and MS. In the study, presented in this paper, we carried out stretching and following compressing experiments on the same samples, with stretching of up to 40%. Rather than reporting the local, microscopic response functions of each SWCNT, we presented the effective conductivity that averages the response over the percolated CNT network. Before being stretched, films showed typical for SWCNT photoconductivity as reported in [18]. The photoconductivity spectra were obtained at $t = 3$ ps pump–probe delay time using the relation described in [17]. As shown in Fig. 2A, the absolute value of the real part of terahertz photoconductivity decreases monotonically with the increasing of the strain in both perpendicular and parallel direction to the probe beam polarization. Photoconductivity changes over stretching and, moreover, is an irreversible feature, which will be indicated further in other characteristics. Full data for all stretching parameters are available in Figs. S3 and S4.

To reveal the nature of change in photoconductivity in the case of the experiments with stretching, we fitted the conductivity of the samples under optical excitation $\sigma_{ex}(\omega)$ and without optical excitation $\sigma_{eq}(\omega)$ with the Drude–Lorentz model for each value of stretching. This model accounts 2 key physical processes, which affect terahertz conductivity: the confined collective motion of carriers along nanotubes (plasmon contribution) and free carrier response, indicative of delocalized intertube transport along percolating channels on a larger scale (Drude contribution) [31,32]. The conductivity in the case of the Drude–Lorentz model reads as follows:

$$\sigma(\omega) = \sigma_D \frac{i\gamma_D}{\omega + i\gamma_D} + \sigma_p \frac{i\omega\gamma_p}{\omega^2 - \omega_0^2 + i\omega\gamma_p}, \quad (1)$$

where σ_D is the DC conductivity of the Drude part, σ_p is the plasmon conductivity at the resonance frequency ω_0 (Lorentz part), and γ_D and γ_p are scattering rates for free-electron and plasmon response, respectively. To understand the spectral dependence, we fitted photoconductivity $\sigma_{ph}(\omega, t) = \sigma_{ex}(\omega) - \sigma_{eq}(\omega)$. We assumed that the plasmonic contribution to the conductivity was unchanged by photoexcitation following our trion interpretation [27]. In detail, this behavior was attributed to the formation of excitons under the photoexcitation prominent in the SWCNT even at room temperature. Therefore, the formation of trions, charged excitons, results in either the removal the charges from the system or the enhancement of the effective masses of such quasiparticles. Hence, to reproduce the negative photoconductivity in our experiments, it needs to be modeled as a drop-in momentum scattering rate accompanied by lower DC conductivity for the Drude model, similar to what has presented in our previous paper.

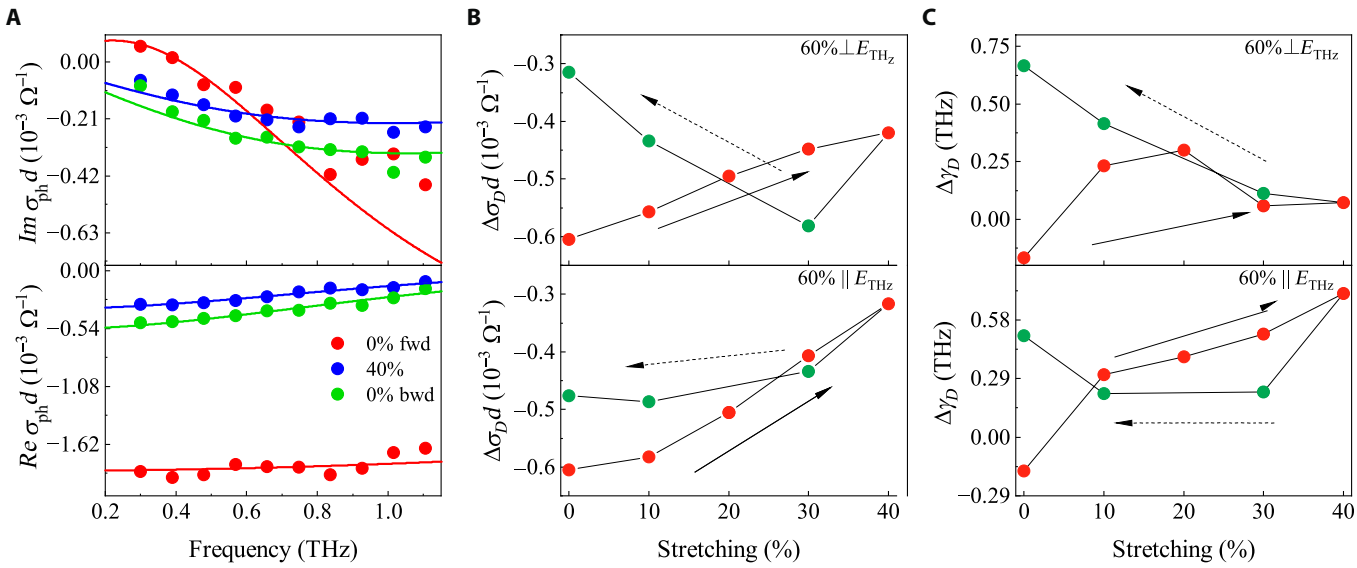

Fig. 2. (A) The film sheet photoconductivity spectra at 3 ps after photoexcitation of the unstretched SWCNT film of 60% transparency ($\epsilon = 0\%$, red color), stretched film ($\epsilon = 40\%$, blue color), and film after compression ($\epsilon = 0\%$, green color), when it is parallel to the polarization of the terahertz radiation. "Fwd" and "bwd" denote the elongation and shrinkage directions of the film, respectively. The change of the DC conductivity (B) and scattering rate (C) obtained from fitting with the change of the Drude model. Red dots in (B) and (C) describe the data in the direction of the film elongation, and the green ones describe the data in the backward compression direction.

We report then the influence of stretching on the change-in-charge carrier transport. As it was mentioned earlier, we considered only the difference between the Drude components of the conductivity in the photoexcited state and equilibrium one. The changes in the fitting parameters $\Delta\sigma_D = \sigma_D^{ex} - \sigma_D^{eq}$ and $\Delta\gamma_D = \gamma_D^{ex} - \gamma_D^{eq}$ in relation to the relative elongation are presented in Fig. 2B and C. At 0 % of stretching, under the optical excitation, the lower change in the DC conductivity accompanied by the reduction of scattering rate was observed. This is consistent with our trion interpretation [27]. The further increase in stretching results in the monotonical decrease of the change in DC conductivity and a higher scattering rate in both parallel and perpendicular directions of the stretching. In terms of free charge behavior, it can be regarded as the lower charge carrier density of free charges under the photoexcitation with a simultaneous decrease in the time between the free charge collisions. This might be interpreted as the decline in the number of the photoinduced charge carriers at high stretching and simultaneous reduction of carriers' mean free path. Moreover, less number of free charges were observed in the perpendicular direction in comparison to the parallel. This is consistent with the possible mechanisms presented in Fig. 1. The formation of microcracks limits the conductivity pathways, resulting in the increase of scattering probability. Moreover, exciton trapping and quenching at cracks result in fewer trion formation and, therefore, less free charges in the system and lower photoconductivity.

The stretching process promotes parallel partial alignment of SWCNT. Because of the anisotropic properties, nanotubes aligned in the same direction as the pump pulse's polarization are preferentially photoexcited. The resulted exciton and, hence, incident terahertz radiation with the same polarization will be absorbed by these carriers. Stretching also might affect the film in a way that parallel to the direction of elongation conductive pathways become longer while perpendicular shorter because of the movement of SWCNT on the contacts and partial alignment.

To evaluate this observation, we also carried out polarization-dependent Raman measurements with a polarizer and parallel analyzer aligned with the direction of elongation and then perpendicular to it, known as VV and HH configurations, respectively. The data for all elongations are shown in Fig. S2. It can be seen that, when the direction of polarization is perpendicular to the direction of stretching, the intensity of the G peak is smaller than when the direction is parallel. This is the signature of the partial alignment shown in [33]: The signal is enhanced when a laser with the polarization parallel to the nanotube's axis was used. The ratio between G mode in perpendicular and parallel direction increased from 0.95 to 1.3 with the increase of the elongation. Moreover, no change of the D to G mode ratio was observed, which suggests the independence of the film elongation to the quality of the sample, particularly to the appearance of defects [33].

Another possible explanation for the change of photoconductivity is the movement of SWCNT on contacts. As the strain increases, the SWCNT and film as a whole experience considerable shrinkage in the parallel direction, and the SWCNT tends to align through sliding. At a certain level of strain, the overall distance between the SWCNTs becomes small enough to form bundles [34,35]. CNTs have a tendency to form bundles that results in lowering conductivity and fewer number of free charges available in the system [28]. This also leads to a fewer trions appearing in the system and, therefore, lower photoconductivity. At large stretching, the bundles are separated into several microblocks with relatively small deformations within these blocks. Once this deformation takes place, the characteristics are irreversible, and diffident trends of photoconductivity are observed in 2 directions. In addition, the sliding of SWCNTs results in a change of the photoconductivity at SWCNT intertube junctions due to the change of the distance between CNTs. Therefore, the change in intertube junctions also results in more packed networks and a change in the photoconductivity.

A more complicated picture was observed in compression experiments. While in the parallel direction, the relative recovery

of the fitting parameters was observed; in the perpendicular direction, the further decrease in photoconductivity and a decrease of the scattering rate were found. This significant difference in the parallel and perpendicular stretching directions suggests that different processes are acquire during the recovery. In particular, the photoconductivity difference along and perpendicular to the stretching direction should be caused by different scattering rates. Moreover, the change in the scattering rate is higher in the perpendicular direction. This indicates the change in the conductivity pathways, which might be explained as the formation of microcracks along the SWCNT and film. Microcracks therefore lead to the scattering from a boundary layer energy barrier, which also modify the charge carrier transport in parallel direction. In addition, in the compression experiments, these microcracks still exist, working as a wire grid polarizer, resulting in higher transparency in the parallel direction and lower in perpendicular. Moreover, the depolarization effect generates lower absorption in a perpendicular direction, which consequently provides lower photoconductivity.

We also would like to point out features at around 0.7 THz for the sample with 90% transparency that were not accounted for by the fitting model, but which has been previously reported [27,36–39] and which may be linked to intraexcitonic transitions (for more details, see Figs. S5 and S6). Importantly, the peak position moves toward higher frequency as the result of stretching. This behavior can be attributed to the influence of defects in electronic band structures and, therefore, in intraexcitonic transitions.

In this section, we show that the stretching of the film leads to the emergence of competing mechanisms of changes in photoconductivity due to morphological modifications, which are connected with the formation of the CNT texture and the growth of the number of microdefects.

Ultrafast optical modulation

The transient phenomena, obtained by varying the time between photoexcitations by OPTP beam, allow for designing a terahertz signal modulator with certain parameters. These modulators are typically characterized by several parameters, among which are MD and MS. MD is defined as follows: $\mathrm{MD} = \Delta E/E_{\mathrm{OFF}} = (E_{\mathrm{ON}} - E_{\mathrm{OFF}})/(E_{\mathrm{OFF}})$, where E_{ON} and E_{OFF} are the detected terahertz signals after the sample with and without optical pump. MD in our experiments depended on several parameters: time delay, frequency, stretching, and pump fluence. To further explore the influence of stretching on ultrafast terahertz modulators, we measured MD as a function of stretching, which varied the optical density in the visible and terahertz ranges simultaneously. The MD of the SWCNT at the peak of the terahertz pulse, which corresponds to a frequency-averaged response as a function of time after photoexcitation in perpendicular and parallel stretching directions toward the polarization of the terahertz beam, is shown in Fig. 3A. As it can be seen, SWCNT film with the transparency of 60% exhibits high MD in the range of nearly 50% to 100%. With an increase in stretching, the MD decreases monotonically from approximately 88% to 55% in parallel direction and from 100% to 70% in perpendicular direction. The modulator reached its highest MD within a few picoseconds before reverting back to its stationary level after approximately 15 ps. It is worth mentioning that the discrepancy between MD in orthogonal directions is connected with the dependence of the extracted photoconductivity on the parameter $\Delta E / E_{\mathrm{OFF}}$ in the approximation of a thin film with a high photoinduced signal [27]. Because photoconductivity is different in these directions, MD differs too.

Here, we defined the maximum operation frequency as $\mathrm{MS} = 1/\tau$ using exponential fits to $\Delta E/E$ with lifetime of the photoinduced charge carriers τ. Modulators, based on the SWCNT of 60% transparency, show a high MS of 205 to 250 GHz, while the MS for a thinner film (with the transparency of 90%, accordingly) varies approximately from 160 to 205 GHz. MS is also irreversible, depending on the orientation, and tends to go backward only halfway from nonstretching to 40%

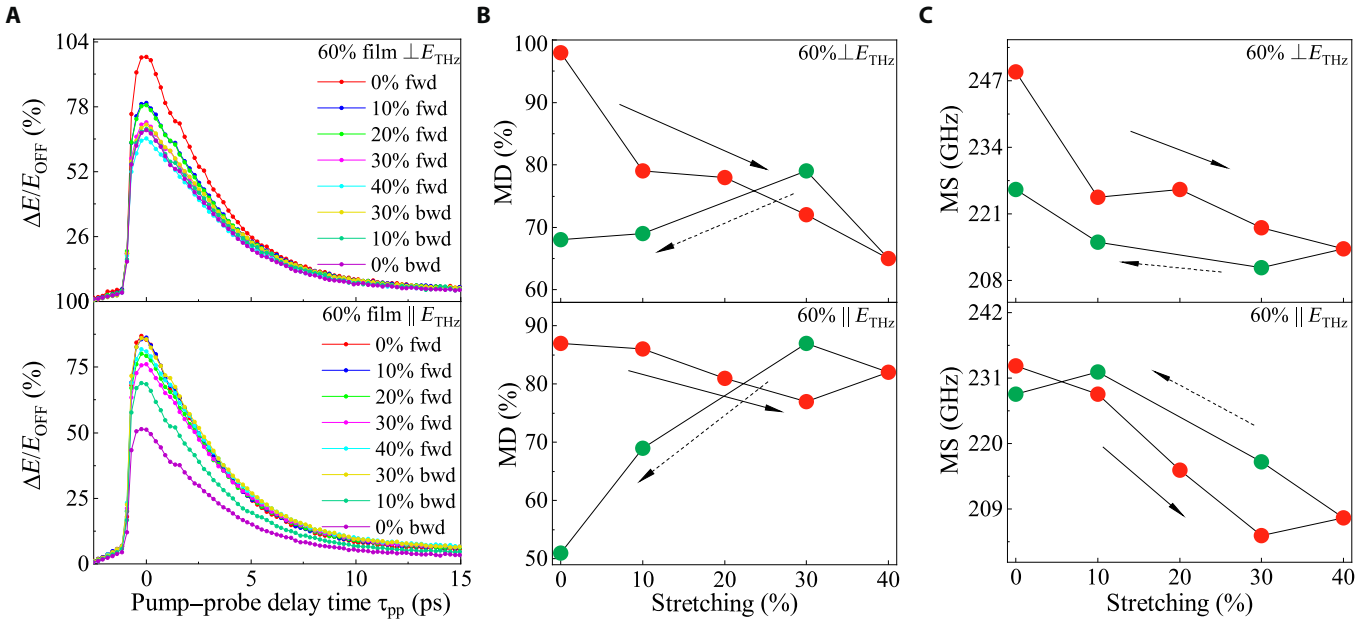

Fig. 3. (A) Modulation depth (MD) in transmission as a function of pump–probe delay time when the elongation is perpendicular (top) and parallel (bottom) to the terahertz probe beam. In transmission mode, MD (B) and modulation speed (MS) (C) for 60% sample at stretching vary from 0% to 40% and at compression from 40% to 0%. The arrows indicate the direction of stretching and the following compression.

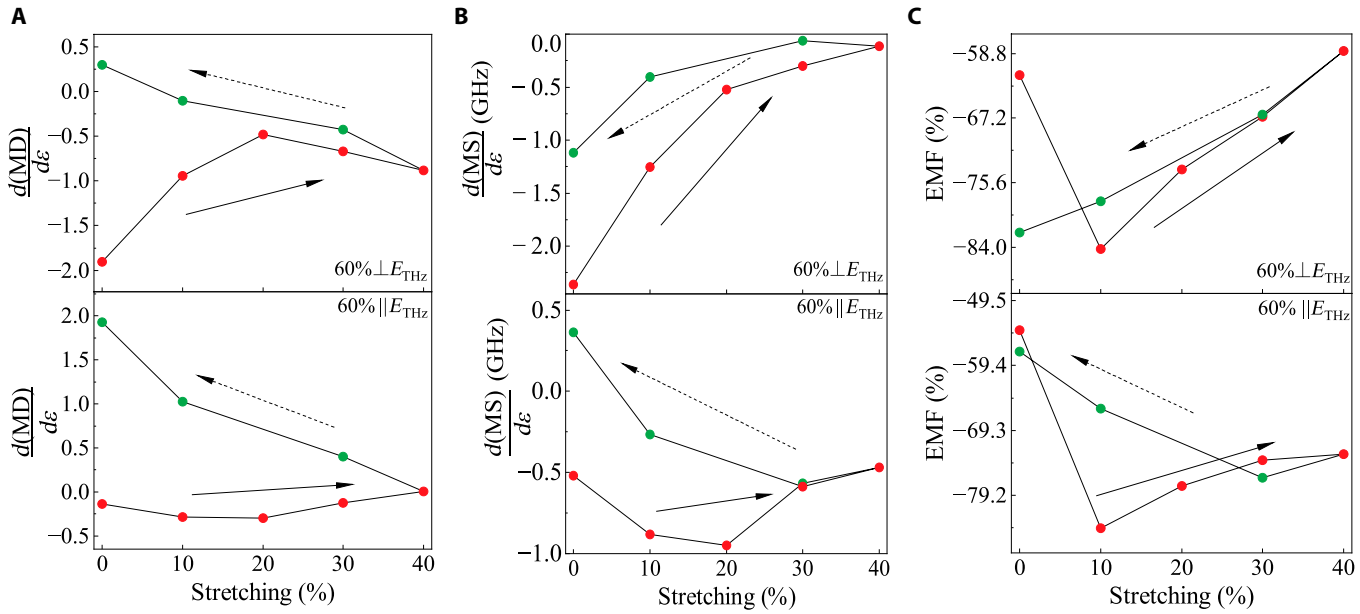

Fig. 4. Strain sensitivity of MD (A), MS (B), and EMF (C) as a function of stretching varies from 0% to 40% and compression from 40% to 0%. The arrows indicate the direction of stretching and following compression.

stretched. Moreover, it is interesting to note that the MS of the films differs, which may be attributed to the different number of charges per unit area in the samples, as it was observed [27].

To understand the dependence of MD and MS on stretching, we plotted the smoothed derivative of both parameters (Fig. 4). Despite the absence of the tendency in the curves, it is seen that the sharpest change in parameters occurs at the very beginning of stretching in most cases. The derivative of the MS increases monotonically with the stretching and slightly recovers in the compression in a perpendicular direction. The maximum value of −2.5 for the MS derivative at 0% means that the MS of the terahertz wave changes by −2.5% for per

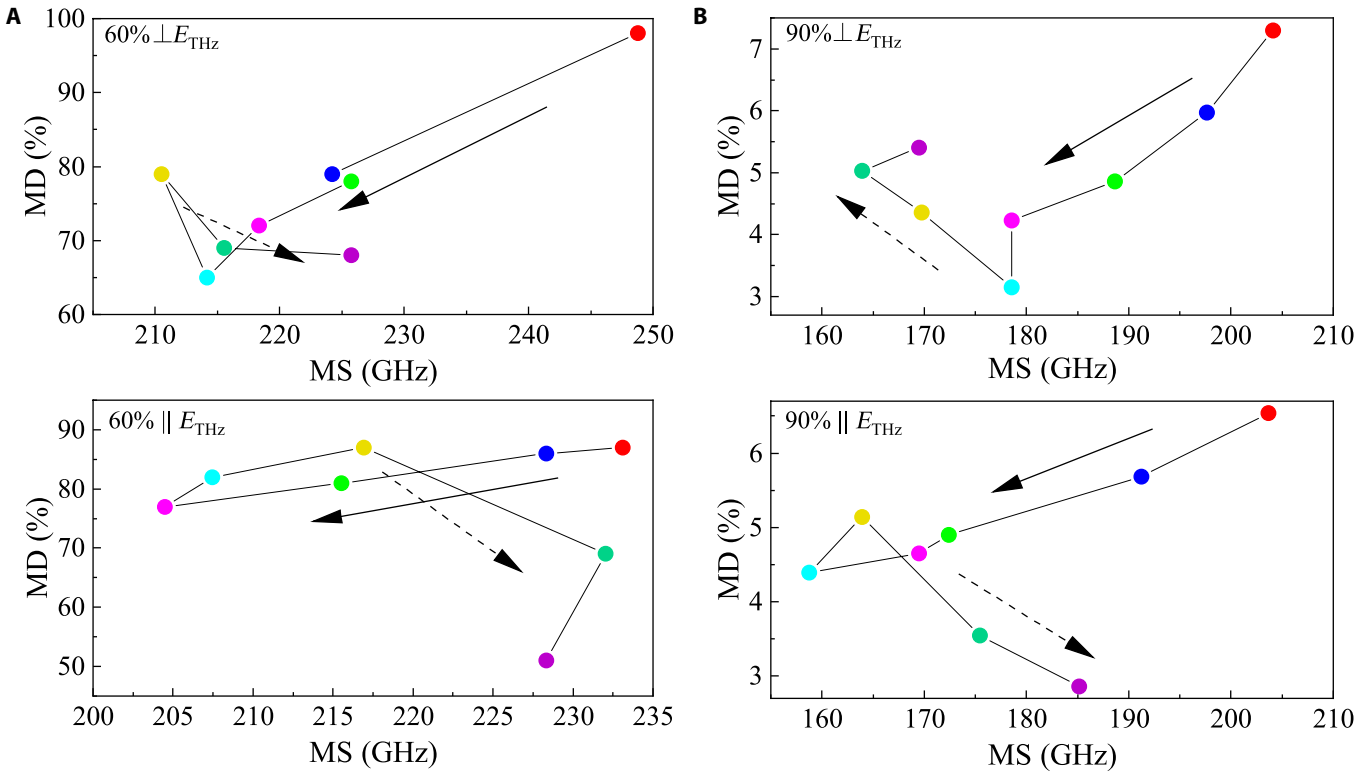

Fig. 5. The frequency-averaged MD (at the peak of the time–domain terahertz pulse) at zero pump–probe delay versus MS for 60% (A) and 90% (B) films at perpendicular and parallel orientation. The colors of the points correspond to the colors in Fig.3A.

change of strain of 1%, while −1 after compression at 0% indicates the −1% change per change of strain 1%. This indicates the deterioration of MS strain sensitivity in the perpendicular direction. Different behaviors were observed in the parallel direction: MS almost recovered after stretching. The derivative for MD shows a value of −2, which also indicates a good initial sensitivity to strain that then switches to 0.5. However, in the parallel direction, it increases from almost 0 to 2.

One more quality of a modulator that was calculated is the EMF (energy modulation factor). It is given by the following formula:

$$\eta = \frac{\int |E_{\mathrm{OFF}}(\omega)|^2 d\omega - \int |E_{\mathrm{ON}}(\omega)|^2 d\omega}{\int |E_{\mathrm{OFF}}(\omega)|^2 d\omega}, \quad (2)$$

where the integration is performed over the range of terahertz pulse frequencies. This metric is a way to evaluate the amount of energy of transmitted terahertz beam when the sample is optically excited compared to the equilibrium case. For normal modulators (based on photoinduced absorption), η is positive, as the energy of the transmitted beam is lower under photoexcitation. SWCNT films with transparency of 60% demonstrate again η varying from −84% to −59%. This indicates that such modulators exhibit high modulation parameters even under significant applied stresses.

As a stretching device, SWCNT thin films can be also characterized by a stretching modulation factor (SMF) defined as follows:

$$\mathrm{SMF} = \frac{\mathrm{MD}(0\%) - \mathrm{MD}(\epsilon = 0...40\%)}{\mathrm{MD}(0\%)}, \quad (3)$$

where MD(0%) is the modulation depth of a nonstretched film. When the elongation reaches 40%, SMF is about 35% in the perpendicular direction and 11% in the parallel direction. At the end of the stretching cycle, it reaches values of 30% and 45% in perpendicular and parallel directions, respectively.

Discussion

In this work, the influence of stretching on optically controlled SWCNT modulators is experimentally demonstrated for the first time. To compare the efficiency of modulation under the applied stretching that was previously reported, we plotted MD versus MS (Fig. 5). First of all, our modulator shows unprecedented, almost 100% MD that is accompanied by a relatively high MS of almost 250 GHz. From one point of view, the tunability can be achived not only optically but also by stretching. Simultaneously, this information can be used to predict the performance of stretchable modulators based on SWCNT. Overall, the deterioration of the MD and MS was observed over the whole stretching circle. The MD exhibit a broad range of values, reaching its minimum of 50% in a parallel direction. A similar situation happens with MS, which reached its minimum value of 205 GHz. We also compared the performance of thicker films with a thinner 90% SWCNT film. Full data are available in Fig. S7. The obtained MD is significantly lower, varying from around 3% to 7%. We also found out that the MD of both films being divided on the thickness of a layer demonstrates almost the same MD, which is a sign of the straight dependence of MD on the film's transparency (and, consequently, thickness). It is seen that MD lessens significantly with stretching in a forward direction up to 40% of its initial length. The backward contraction reveals that MD before and after stretching is different, which reflects irreversible properties of SWCNT photoconductivity.

We have demonstrated the influence of stretching on terahertz photoconductivity and performance of optically controlled terahertz modulators based on macroscale SWCNT films. The high tunability of the modulator parameters over the full stretching circle was presented for SWCNT films on a stretchable substrate. The MD is continuously tuned from 100% to 70% under stretching from 0% to 40%. The MS is changing from 250 to 205 GHz. The physical mechanism of such behavior is discussed in terms of the change of photoconductivity due to morphology change. A flexible broadband terahertz modulator based on a strain-sensitive SWCNT film is reported. As a conclusion, we would like to point out that the optical control of the proposed modulator allows to reach ultrafast operation frequencies, while its mechanical control enables the possibility to set MD and MS, which are required for the communication system working at a particular speed.

Acknowledgments

We would like to thank the Warwick Centre for Ultrafast Spectroscopy (University of Warwick, UK) for access to the OPTP spectrometer used. **Funding:** M.G.B. and M.I.P. acknowledge Russian Science Foundation (RSF) project no. 21-79-10097 (experimental OPTP measurements) and Ministry of Science and Higher Education of the Russian Federation no. 0714-2020-0002 (anisotropy factor measurements for SWCNT films). Moreover, M.G.B. acknowledges RSF project no. 22-72-10033 (investigation of the stretchable modulators efficiency). B.P.G. and A.G.N. acknowledge RSF project no. 21-72-20050 (sample preparation). **Competing interests:** The authors declare that they have no known competing financial interests or personal relationships that could have appeared to influence the work reported in this paper.

Data Availability

The data that support the plots within this article and other findings of this study are available from the corresponding author upon reasonable request.

Supplementary Materials

Fig. S1. The anisotropy factor for SWCNT films with different transparencies.
Fig. S2. Raman spectra of SWCNT films at different stretching.
Figs. S3–S6. Photoconductivity spectra for all samples, positions of the samples towards THz polarization, and all stretching deformations.
Fig. S7. The same as Fig. 3 for the sample with a transparency of 90%.

References

1. Federici JF, Schulkin B, Huang F, Gary D, Barat R, Oliveira F, Zimdars D. THz imaging and sensing for security applications—Explosives, weapons and drugs. *Semicond Sci Technol*. 2005;20(7):S266–S280.
2. Zaytsev KI, Kudrin KG, Karasik VE, Reshetov IV, Yurchenko SO. In vivo terahertz spectroscopy of pigmentary skin nevi: Pilot study of non-invasive early diagnosis of dysplasia. *Appl Phys Lett*. 2015;106(5):Article 053702.

3. Zeitler J, Gladden L. In-vitro tomography and non-destructive imaging at depth of pharmaceutical solid dosage forms. *Eur J Pharm Biopharm*. 2009;71(1):2–22.
4. Miles RE, Zhang X-C, Eisele H, Krotkus A. *Terahertz frequency detection and identification of materials and objects.* Dordrecht (Netherlands): Springer Netherlands; 2007.
5. Federici J, Moeller L. Review of terahertz and subterahertz wireless communications. *J Appl Phys*. 2010;107(11):Article 111101.
6. Sarieddeen H, Saeed N, Al-Naffouri TY, Alouini M-S. Next generation terahertz communications: A rendezvous of sensing, imaging, and localization. *IEEE Commun Mag*. 2020;58(5):69–75.
7. Rahm M, Li J-S, Padilla WJ. THz wave modulators: A brief review on different modulation techniques. *J Infrared Millim Terahertz Waves*. 2013;34:1–27.
8. Beard MC, Turner GM, Schmuttenmaer CA. Subpicosecond carrier dynamics in low-temperature grown GaAs as measured by time-resolved terahertz spectroscopy. *J Appl Phys*. 2001;90(12):5915–5923.
9. Chen Z, Chen X, Tao L, Chen K, Long M, Liu X, Yan K, Stantchev RI, Pickwell-MacPherson E, Xu J-B. Graphene controlled Brewster angle device for ultra broadband terahertz modulation. *Nat Commun*. 2018;9:4909.
10. Kersting R, Strasser G, Unterrainer K. Terahertz phase modulator. *Electron Lett*. 2000;36(13):1156–1158.
11. Kleine-Ostmann T, Dawson P, Pierz K, Hein G, Koch M. Room-temperature operation of an electrically driven terahertz modulator. *Appl Phys Lett*. 2004;84(18):3555–3557.
12. Cheng L, Jin Z, Ma Z, Su F, Zhao Y, Zhang Y, Su T, Sun Y, Xu X, Meng Z, et al. Mechanical terahertz modulation based on single-layered graphene. *Adv Opt Mater*. 2018;6(7):1700877.
13. Liu J, Li P, Chen Y, Song X, Mao Q, Wu Y, Qi F, Zheng B, He J, Yang H, et al. Flexible terahertz modulator based on coplanar-gate graphene field-effect transistor structure. *Opt Lett*. 2016;41(4):816–819.
14. Kharlamova MV, Burdanova MG, Paukov MI, Kramberger C. Synthesis, sorting, and applications of single-chirality single-walled carbon nanotubes. *Materials*. 2022;15(17):5898.
15. Kharlamova MV, Paukov M, Burdanova MG. Nanotube functionalization: Investigation, methods and demonstrated applications. *Materials*. 2022;15(15):5386.
16. Gilshteyn EP, Romanov SA, Kopylova DS, Savostyanov GV, Anisimov AS, Glukhova OE, Nasibulin AG. Mechanically tunable single-walled carbon nanotube films as a universal material for transparent and stretchable electronics. *ACS Appl Mater Interfaces*. 2019;11(30):27327–27334.
17. Burdanova MG, Tsapenko AP, Kharlamova MV, Kauppinen EI, Gorshunov BP, Kono J, Lloyd-Hughes J. A review of the terahertz conductivity and photoconductivity of carbon nanotubes and heteronanotubes. *Adv Opt Mater*. 2021;9(24):Article 2101042.
18. Burdanova MG, Katyba GM, Kashtiban R, Komandin GA, Butler-Caddle E, Staniforth M, Mkrtchyan AA, Krasnikov DV, Gladush YG, Sloan J, et al. Ultrafast, high modulation depth terahertz modulators based on carbon nanotube thin films. *Carbon*. 2021;173:245–252.
19. Kar S, Lake J, Adeyemo S, Santra T, Joyce H. The physics of terahertz negative photoconductivity in low-dimensional materials. *Mater Today Phys*. 2022;23:100631.
20. Xu S-T, Mou L-L, Fan F, Chen S, Zhao Z, Xiang D, de Andrade MJ, Liu Z, Chang S-J. Mechanical modulation of terahertz wave via buckled carbon nanotube sheets. *Opt Express*. 2018;26(22):28738–28750.
21. Gubarev V, Yakovlev VY, Sertsu MG, Yakushev OF, Krivtsun VM, Gladush YG, Ostanin IA, Sokolov A, Schäfers F, Medvedev VV, et al. Single-walled carbon nanotube membranes for optical applications in the extreme ultraviolet range. *Carbon*. 2019;155:734.
22. Khabushev EM, Krasnikov DV, Zaremba OT, Tsapenko AP, Goldt AE, Nasibulin AG. Machine learning for tailoring optoelectronic properties of single-walled carbon nanotube films. *J Phys Chem Lett*. 2019;10(21):6962–6966.
23. Khabushev EM, Krasnikov DV, Kolodiazhnaia JV, Bubis AV, Nasibulin AG. Structure-dependent performance of single-walled carbon nanotube films in transparent and conductive applications. *Carbon*. 2020;161:712–717.
24. Kaskela A, Nasibulin AG, Timmermans MY, Aitchison B, Papadimitratos A, Tian Y, Zhu Z, Jiang H, Brown DP, Zakhidov A, et al. Aerosol-synthesized SWCNT networks with tunable conductivity and transparency by a dry transfer technique. *Nano Lett*. 2010;10(11):4349–4355.
25. Nasibulin AG, Moisala A, Brown DP, Jiang H, Kauppinen E. A novel aerosol method for single walled carbon nanotube synthesis. *Chem Phys Lett*. 2005;402(1–3):227–232.
26. Monti M, Tao SX, Staniforth M, Crocker A, Griffin E, Wijesekara A, Hatton RA, Lloyd-Hughes J. Efficient Intraband hot carrier relaxation in the perovskite semiconductor $Cs_{1-x}Rb_xSnI_3$ mediated by strong electron-phonon coupling. *J Phys Chem C*. 2018;122(36):20669–20675.
27. Burdanova MG, Tsapenko AP, Satco DA, Kashtiban R, Mosley CDW, Monti M, Staniforth M, Sloan J, Gladush YG, Nasibulin AG, et al. Giant negative terahertz photoconductivity in controllably doped carbon nanotube networks. *ACS Photonics*. 2019;6(4):1058–1066.
28. Shuba MV, Paddubskaya AG, Kuzhir PP, Slepyan GY, Seliuta D, Kašalynas I, Valušis G, Lakhtakia A. Effects of inclusion dimensions and p-type doping in the terahertz spectra of composite materials containing bundles of single-wall carbon nanotubes. *J Nanophoton*. 2012;6(1):Article 061707.
29. Shindo Y, Kuronuma Y, Takeda T, Narita F, Fu S-Y. Electrical resistance change and crack behavior in carbon nanotube/polymer composites under tensile loading. *Compos Part B*. 2012;43(1):39–43.
30. Islam MF, Milkie DE, Kane CL, Yodh AG, Kikkawa JM. Direct measurement of the polarized optical absorption cross section of single-wall carbon nanotubes. *Phys Rev Lett*. 2004;93(3):Article 037404.
31. Zhukova ES, Grebenko AK, Bubis AV, Prokhorov AS, Belyanchikov MA, Tsapenko AP, Gilshteyn EP, Kopylova DS, Gladush YG, Anisimov AS, et al. Terahertz-infrared electrodynamics of single-wall carbon nanotube films. *Nanotechnology*. 2017;28(44):Article 445204.
32. Gorshunov B, Zhukova ES, Starovatykh JS, Belyanchikov MA, Grebenko AK, Bubis AV, Tsebro VI, Tonkikh AA, Rybkovskiy DV, Nasibulin AG, et al. Terahertz spectroscopy of charge transport in films of pristine and doped single-wall carbon nanotubes. *Carbon*. 2018;126:544–551.
33. Fischer D, Pötschke P, Brünig H, Janke A. Investigation of the orientation in composite fibers of polycarbonate with multiwalled carbon nanotubes by raman microscopy. *Macromol Symp*. 2005;230(1):167–172.

34. Liu Q, Li M, Gu Y, Zhang Y, Wang S, Li Q, Zhang Z. Highly aligned dense carbon nanotube sheets induced by multiple stretching and pressing. *Nanoscale*. 2014;6(8):4338–4344.
35. Nam TH, Goto K, Yamaguchi Y, Premalal EVA, Shimamura Y, Inoue Y, Arikawa S, Yoneyama S, Ogihara S. Improving mechanical properties of high volume fraction aligned multi-walled carbon nanotube/epoxy composites by stretching and pressing. *Compos Part B*. 2016;85:15–23.
36. Kar S, Sood A. Ultrafast terahertz photoresponse of single and double-walled carbon nanotubes: Optical pump-terahertz probe spectroscopy. *Carbon*. 2019;144:731–736.
37. Xu X, Chuang K, Nicholas RJ, Johnston MB, Herz LM. Terahertz excitonic response of isolated single-walled carbon nanotubes. *J Phys Chem C*. 2009;113(42):18106–18109.
38. Lui CH, Frenzel AJ, Pilon DV, Lee Y-H, Ling X, Akselrod GM, Kong J, Gedik N. Trion-induced negative photoconductivity in monolayer MoS_2. *Phys Rev Lett*. 2014;113:Article 166801.
39. Luo L, Liu Z, Yang X, Vaswani C, Cheng D, Park JM, Wang J. Anomalous variations of spectral linewidth in internal excitonic quantum transitions of ultrafast resonantly excited single-walled carbon nanotubes. *Phys Rev Mater*. 2019;3:Article 026003.